Journal of Chromatography A, 1223 (2012) 24–34

Contents lists available at SciVerse ScienceDirect

Journal of Chromatography A

journal homepage: www.elsevier.com/locate/chroma

A molecular simulation study of the effects of stationary phase and solute chain length in reversed-phase liquid chromatography

Jake L. Rafferty[a,b], J. Ilja Siepmann[a,c,*], Mark R. Schure[d]

[a] Department of Chemistry and Chemical Theory Center, University of Minnesota, 207 Pleasant Street SE, Minneapolis, MN 55455-0431, USA
[b] Department of Chemistry, North Hennepin Community College, 7411 85th Avenue North, Brooklyn Park, MN 55445, USA
[c] Department of Chemical Engineering and Materials Science, University of Minnesota, 421 Washington Avenue SE, Minneapolis, MN 55455-0132, USA
[d] Theoretical Separation Science Laboratory, The Dow Chemical Company, 727 Norristown Road, Box 0904, Spring House, PA 19477-0904, USA

ARTICLE INFO

Article history:
Received 4 August 2011
Received in revised form
17 November 2011
Accepted 20 November 2011
Available online 25 November 2011

Keywords:
Reversed-phase liquid chromatography
Retention mechanism
Molecular simulation
Chain length
Hydrophilic interaction liquid chromatography

ABSTRACT

The effects of stationary phase and solute chain length are probed by carrying out Monte Carlo simulations of dimethyl triacontyl (C_{30}), dimethyl octadecyl (C_{18}), dimethyl octyl (C_8), and trimethyl (C_1) silane grafted, and bare silica stationary phases in contact with a water/methanol mobile phase and by examining the retention of solutes from 1 to 14 carbons in length. Fairly small differences in structure are observed when comparing the C_{30}, C_{18}, C_8 systems and the retention mechanism of nonpolar alkane solutes shows contribution from both partitioning and adsorption on all three of these stationary phases. Unlike in the other systems, the mobile phase solvent is highly structured at its interface with the C_1 and bare silica phases, the former being enriched in methanol and the latter in water. Alkane solutes are unretained at the bare silica surface while alcohol solutes are only slightly enriched at the silica surface due to hydrogen bonding with surface silanols and surface bound solvent. With regard to solute size, it appears that the retention mechanism is not affected by the chain length of the solute.

1. Introduction

Reversed-phase liquid chromatography (RPLC) is an extremely versatile and widely used technique for chemical separations, purifications, and analyses. One of the powerful aspects of the RPLC technique is the number of chromatographic parameters that can be adjusted in order to achieve the desired selectivity and/or efficiency for a given a separation. However, a molecular-level description of how changes in these parameters lead to changes in retention and selectivity remains lacking for many RPLC systems [1]. A better understanding of these parameters should aid in the optimization of current RPLC systems and in the development of new separation technologies.

Particle-based simulations have been employed by a few research groups to study structural, dynamic, and thermodynamic properties of RPLC systems [2–13]. It has been the ongoing goal of this research group to systematically investigate various chromatographic parameters including retention mechanisms using advanced molecular simulation techniques that allow for a molecular-level viewpoint. In previous reports we have detailed the effects of solvent composition [14–17], grafting density [18,19], polar-embedded groups [20], pressure [21], and pore shape [21] on the structure of the RPLC stationary phase and on the molecular mechanism of retention. In the current work, we examine what effect the length of the alkyl chains in the stationary phase has on structure and retention in RPLC and also if the solute chain length plays any role in altering the retention mechanism.

The two most popular stationary phase chain lengths used in RPLC are C_8 and C_{18}; however, numerous studies of chain lengths ranging from C_1 to over C_{30} have appeared in the literature. Generally, it is observed that retention increases, but selectivity is little affected with increasing stationary phase chain length [22–29]. However, it should be noted that the selectivity between geometrically constrained solutes, such as polycyclic aromatic hydrocarbons, can increase with longer chain lengths which has been used to infer that the longer chains are more conformationally ordered [30]. This increased order has been confirmed through spectroscopic measurements [31–34].

With regard to solute chain length, it has been observed from retention measurements with various homologous series (for example normal alkanes or alcohols with varying chain length) that retention increases with increasing solute length, but there is a break in the slope in plots of $\log k'$ versus number of carbons [27,35,36]. This break occurs about where the number of carbons

* Corresponding author at: Department of Chemistry and Chemical Theory Center, University of Minnesota, 207 Pleasant Street SE, Minneapolis, MN 55455-0431, USA. Tel.: +1 612 624 1844.
E-mail address: siepmann@umn.edu (J.I. Siepmann).

0021-9673/$ – see front matter © 2011 Elsevier B.V. All rights reserved.
doi:10.1016/j.chroma.2011.11.039

in the solute exceeds the number of carbons in the stationary phase chains. From this observation it was suggested that the solutes fully embed themselves (partition) into the stationary phase until their length exceeds the length of the stationary phase and, after this, the remaining portion of the solute is forced to reside outside the stationary phase and adsorb at the surface. However, a regular curvature has been observed in plots of log k' versus homolog number in some cases [37].

In the present study, Gibbs ensemble simulations using efficient configurational-bias Monte Carlo (CBMC) algorithms and transferable force fields were carried out to probe chain length effects in RPLC. The structural properties and retention behavior were investigated for five stationary phases differing in the length of the alkyl silane ligand (C_{30}, C_{18}, C_8, C_1, and bare silica). The effects of solute chain length (ranging from ethane to tetradecane) on the retention mechanism were studied for the C_8 stationary phase.

2. Simulation details

To examine the effects of chain length in RPLC, coupled–decoupled configurational-bias Monte Carlo simulations (CBMC) [38–41] in the isobaric–isothermal version of the Gibbs ensemble [42] are employed. The simulations make use of three separate simulation boxes that are in thermodynamic contact but do not share an explicit interface. The first simulation box is elongated with $L_x = 20.0$ Å, $L_y = 26.0$ Å, $L_z = 90.0$ Å. The center of this box contains a silica slab consisting of five layers of β-cristobalite with its two (1 1 1) surfaces exposed in the x–y plane. In one set of simulations the silanols on these two surfaces were left unreacted, whereas in the other sets of simulations these surfaces were modified by the grafting of trimethyl (C_1), dimethyl octylsilane (C_8), dimethyl octadecylsilane (C_{18}), or dimethyl triacontylsilane chains (C_{30}) at a density of 2.9 μmol/m^2 (9 chains on each surface) resulting in a residual silanol density of 4.8 μmol/m^2 (15 silanols on each surface). In each of these four systems, the silane chains were placed in the exact same surface arrangement. In contact with this stationary phase, and connected through the periodic boundaries used in the simulations, is the mobile phase solvent. Thus, the setup in this first box corresponds to a planar slit pore. Snapshots from the simulations of each system showing one of the silica surfaces in contact with the mobile phase solvent are presented in Fig. 1.

The second simulation box contains a bulk mobile phase reservoir and the third box a helium vapor phase. These boxes are cubic and their volumes are allowed to fluctuate in response to the external pressure. The simulations probing the effects of changes in the bonded-phase chain length were carried out at a temperature of 323 K and a pressure of 10 atm. For these simulations, the mobile phase consisted of a water/methanol mixture containing 33% molfraction (≈50% volume fraction) methanol and the probe solutes utilized were C_1 to C_4 normal alkanes and alcohols. For the studies of solute chain length only the C_8 stationary phase was examined; the mobile phase consisted of 67% molfraction (≈80% volume fraction) methanol, the temperature was 298 K, the pressure was 10 atm, and the probe solutes were normal alkanes solutes up to 14 carbons in length. A detailed description of the simulation setup and methodology and a discussion on the merits of a three-box Gibbs ensemble setup can be found in a recent review article [43].

To describe the intra- and intermolecular interactions in the model RPLC systems, the TIP4P model [44] was used for water, the silica substrate was represented by a zeolite potential with Lennard–Jones sites on oxygen atoms [45] and explicit charges on silicon, oxygen, and the dangling hydrogens [46,47], and the interactions of all other species (methanol, alkyl ligands, and alkane and alcohol solutes) were described by the united-atom version of the transferable potentials for phase equilibria (TraPPE) force field [47,48]. Lennard–Jones interactions were truncated at 10 Å and Coulomb interactions were evaluated with the Ewald summation technique [49] using a direct space cutoff of 10 Å and a convergence parameter of $\kappa = 0.28$. The alkyl ligands, solute molecules, and methanol were treated as semi-rigid species with allowance for bond angle bending and dihedral motion but the bond length being kept rigid, whereas water molecules were kept rigid.

For each model RPLC system, eight independent simulations were carried out. Each independent simulation was equilibrated for at least 2×10^5 Monte Carlo (MC) cycles followed by an additional 5×10^5 MC cycles for production. One MC cycle corresponds

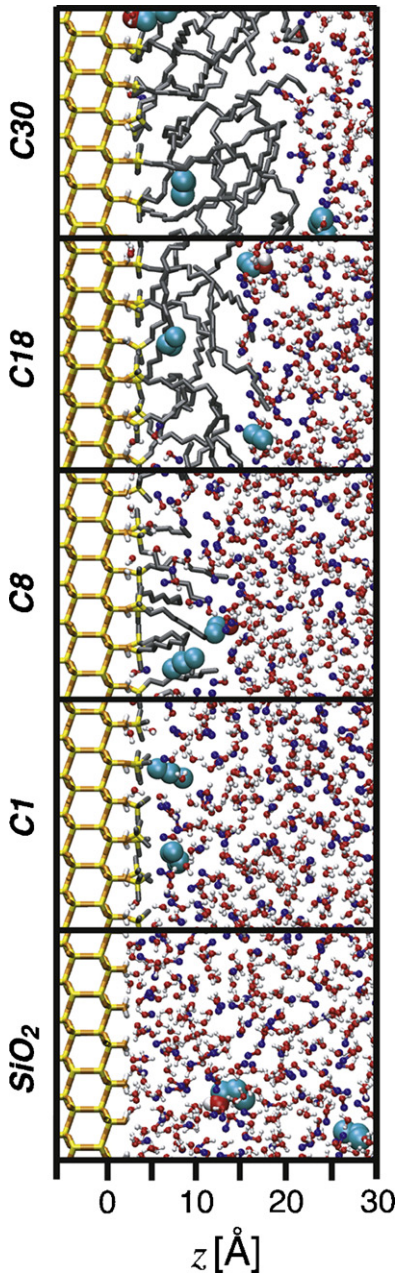

Fig. 1. Simulations snapshots of the five systems. The stationary phase is shown as tubes with silicon in yellow, oxygen in orange, hydrogen in white and carbon in black. The mobile phase is shown in the ball and stick representation with oxygen in red, hydrogen in white, and carbon in blue. The analyte molecules are depicted by large spheres with oxygen in red, hydrogen in white, and carbon in cyan. (For interpretation of the references to color in this figure legend, the reader is referred to the web version of the article.)

Table 1
Structural properties for systems with different alkylsilane chain lengths.[a]

System	f_{gauche}	S_n	$\cos\theta_{ete}$	z_{CH_3} (Å)	z_{GDS} (Å)	$\delta_{interface}$ (Å)
C_{30}	0.27_1	0.00_1	0.51_2	14.6_3	21.8_1	5.8_2
C_{18}	0.27_1	-0.05_1	0.43_3	10.9_3	14.8_2	5.3_4
C_8	0.28_1	0.17_1	0.68_1	9.4_1	10.3_1	7.4_3
C_1[b]	–	–	0.68_1	4.4_1	6.2_1	3.0_1

[a] Subscripts indicate the statistical uncertainty in the final digit. Values of f_{gauche} and S_n for C_{18} and C_8 systems differ slightly from those reported in Ref. [21] because the Si-C-C-C dihedral angle and the Si-C-C 1–3 backbone vector are not included in the analysis here.
[b] For the C_1 phase, values of $\cos\theta_{ete}$ and z_{CH_3} were calculated for the outermost CH_3 group.

to N MC moves, where N is the number of molecules in the three-phase system. Statistical uncertainties in the reported quantities were estimated from the standard error of the mean of the results from the eight independent simulations. A very detailed description of the system setup and equilibration protocols, the selection of Monte Carlo moves, and the analysis methods for these simulations can found in two recent articles [43,50] and, hence, is not repeated here.

3. Results and discussion

3.1. Effects of stationary phase chain length

3.1.1. Chain order

The different retention behavior of various alkyl silane stationary phases is related to differences in structural characteristics, such as the degree of order/disorder in the tethered alkyl chains. Typically, the measurement of order in the stationary phase is carried out through spectroscopic analysis [34], but it is also often inferred through retention measurements. Molecular simulation is also a very useful tool for this purpose. Atomic coordinates from a simulation can be used to exactly pinpoint specific chain conformations and one can directly measure a wide variety of structural properties in a single simulation.

A summary of the conformational properties of the stationary phases examined in this work is presented in Table 1. The first entry in this table is the fraction of gauche defects (f_{gauche}), or fraction of dihedral angles in the entire chain deviating by more than 60° from the angle of the trans conformer. Our results indicate the fraction of gauche defects is similar for C_{30} and C_{18} phases at 0.27, and there are slightly more gauche defects in the C_8 phase. An increase in gauche defects with decreasing chain length has been observed through FTIR [33], Raman [31,32], and NMR [34] spectroscopic measurements. Singh et al. observed gauche defect fractions of about 0.1, 0.2, and 0.4 for C_{30}, C_{18}, and C_8 phases, respectively, but these FTIR measurements were done for polymeric phases with much higher densities than the monomeric phases studied here [33]. A gauche fraction of 0.28 was also observed for bulk liquid *n*-octadecane and an isolated *n*-octadecane chain solvated in methanol [51].

The simulations allow one to not only measure the fraction of gauche defects for the entire chain, but also at each dihedral bond center along the chain backbone (see Fig. 2). For segments near the silica surface, there is a similar oscillating pattern of gauche defects for the C_{30}, C_{18}, and C_8 chain systems, likely caused by packing constraints near the surface. Additionally, all three phases show a large fraction of gauche defects at the free chain end. Interestingly, the fraction of gauche defects is relatively constant at around 0.27 between dihedrals 15 and 25 for the C_{30} phase, suggesting a liquid-like state in this region of the phase [51].

Another characterization of chain structure is the order parameter S, which is equivalent to the NMR order parameter for deuterated alkyl chains [52] and is defined as

$$S_i = \frac{1}{2}\langle 3\cos^2\theta_i - 1\rangle \quad (1)$$

where θ_i is the angle between the ith 1–3 backbone vector in the alkyl chain (between carbons separated by two bonds) and the normal to the silica substrate. This order parameter approaches unity for vectors preferentially aligned perpendicular to the surface, −0.5 for parallel vectors, and vanishes if there is no preferential orientation (or for a very narrow distribution around the magic angle). When averaged over the entire chain, the values for this order parameter (see Table 1) do not follow a distinct trend with chain length and are positive for the C_8 phase, suggesting a preference for alignment perpendicular to the silica surface, and slightly negative for the C_{18} phase, suggesting a slight preference for parallel alignment. This is contrary to what one would typically expect, i.e., that the shorter chains are less ordered, but can be rationalized by examining the order parameter at each position along the chain backbone (Fig. 2). For all chain lengths, the lower portion of the chains exhibits positive S values (with the value largest for the part next to the silane linker), and these values do not become negative until about the seventh 1–3 segment. However, the C_8 chain only has six 1–3 vectors and never reaches the point where the order parameter becomes negative. The plots of the order parameter for the C_{18} and C_{30} phases are qualitatively similar, reaching a minimum about two-thirds of the way along the chain. However, the C_{30} chains show slightly higher S values along the entire chain, indicating less of a preference to be parallel to the silica surface.

Chain alignment can also be characterized through $\cos\theta_{ete}$, the cosine of the angle between the chain's end-to-end vector (from

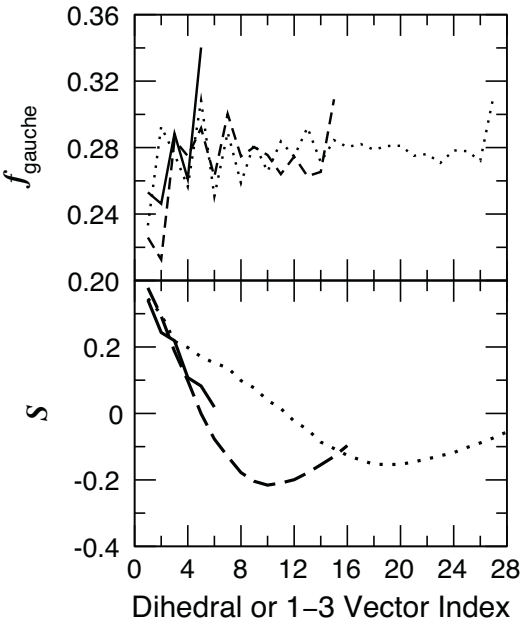

Fig. 2. Fraction of gauche defects (upper) and order parameter (lower) along the chain backbone. The C_8, C_{18}, and C_{30} phases are shown as solid, dashed and dotted lines, respectively. The index 1 is used for the dihedral angle and the 1–3 vector closest to the silicon atom of the alkyl silane. Hence, the index for the terminal dihedral angle of an *n*-alkyl ligand is given by $n-3$.

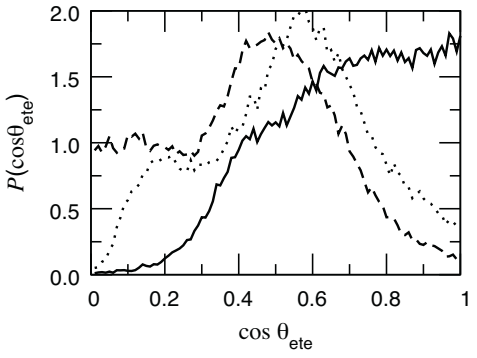

Fig. 3. Distribution of chain end-to-end angles. Line styles as in Fig. 2.

the tertiary silicon atom to the terminal methyl group) and the normal to the silica substrate, or the tilt angle. The value of $\cos\theta_{ete}$ can range from 0 for chains oriented parallel to the silica surface to 1 for chains perpendicular to the silica surface. The average value of $\cos\theta_{ete}$ is presented in Table 1 while its distribution is shown in Fig. 3. For the stationary phases studied here, average $\cos\theta_{ete}$ values are largest for the C_8 phase and smallest for the C_{18} phase, indicating that the C_8 phase has the strongest preference to align perpendicular to the silica surface. The distribution of $\cos\theta_{ete}$ for the C_{18} and C_{30} chains show peaks around 0.5 and 0.6, respectively, but also have significant probabilities for chains with much smaller $\cos\theta_{ete}$ values, i.e., chains more parallel to the silica surface. For the C_8 phase the distribution is shifted to larger $\cos\theta_{ete}$ values and there is a very low probability for chains with small $\cos\theta_{ete}$ values. Taken together with the *S* values along the chain backbone, this indicates that the C_8 chains possess the most alignment because, due to their shorter length, they are not able to backfold while a longer chain can.

To summarize the effect of chain length on stationary phase structure, it appears that chains in the C_8 phase show the most alignment but largest degree of conformational disorder (gauche defects). The C_{30} and C_{18} phases show similar degrees of conformational order, but the C_{30} phase has a higher degree of alignment (larger *S* and $\cos\theta_{ete}$ values). It should be emphasized here that these results pertain to monomeric bonded phases with intermediate coverage and that much higher grafting densities lead to significant changes in the chain alignment [18].

3.1.2. Local composition and stationary phase thickness

Another way to gain insight on the mechanism of solute retention and the origins of selectivity is to examine the local composition of each system as one moves from the mobile and into the stationary phase. For this purpose, density profiles for water, methanol, and stationary phase carbon atoms are presented in Fig. 4 as a function of distance from the silica substrate (*z*, see Fig. 1). These plots also show the Gibbs dividing surface (GDS, a plane defining the border between the mobile and stationary phases [53,54]) and the width of the interfacial region, which is defined as the range where the total solvent density falls between 10% and 90% of its bulk value. The GDS and interfacial width are fit to the total solvent density using a hyperbolic tangent method [55]. Numerical values for the GDS and interfacial width, z_{GDS} and $\delta_{interface}$, are given in Table 1. It is not possible to define a GDS and interfacial region for the bare SiO_2 system because of large oscillations in the total solvent density near the silica surface.

Starting in the mobile phase solvent and moving towards the stationary phase chains one notices a number of similarities between the alkylsilane systems. First, one observes a peak in the methanol density profile just above the location of the GDS, whereas the water density falls smoothly as the GDS is approached

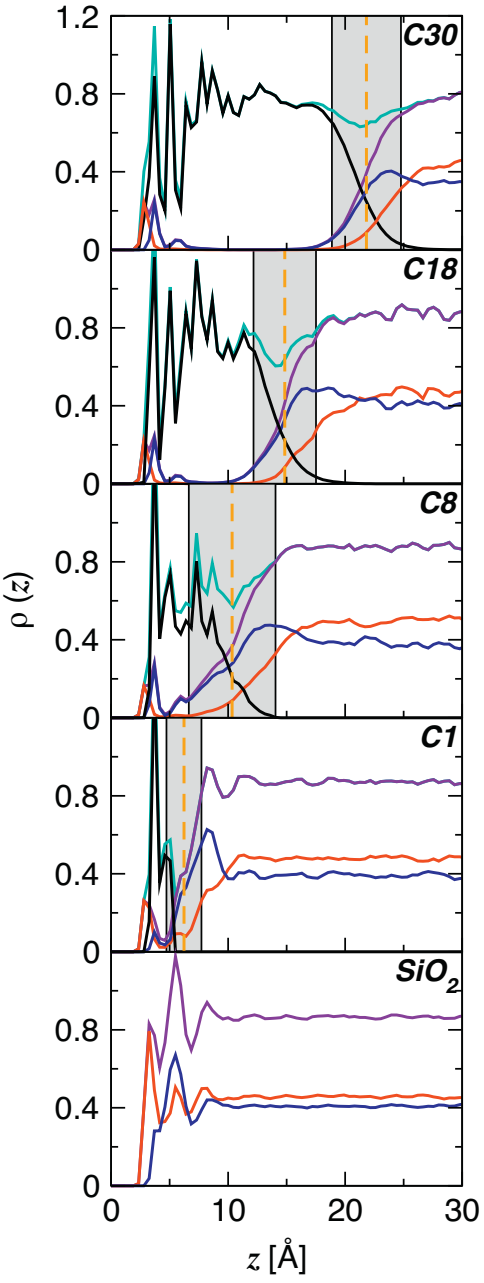

Fig. 4. System composition as a function of distance from the silica surface (*z*, defined in Fig. 1). Stationary phase carbon density is shown in black, methanol in blue, and water in red. The total system and solvent densities are shown in cyan and purple, respectively. The GDS is shown by the orange dashed line and the interfacial region is shaded gray. (For interpretation of the references to color in this figure legend, the reader is referred to the web version of the article.)

from above, i.e., there is a significant enrichment of the organic modifier in this region that extends deep into the interior of the bonded-chain region [14,17]. The amount of methanol enrichment at the surface appears to be roughly similar in all four alkylsilane systems. This is in agreement with the work of Kazakevich et al., who measured the excess adsorption isotherms of methanol from water on alkylsilane stationary phases with different chain lengths [57]. Second, there is a depletion of the total system density for all four alkyl silane phases (see cyan lines in Fig. 4), i.e., a dewetting effect at the hydrophobic surface [56].

Although the same general features are seen at the interface regardless of chain length, there are some differences between the

Table 2
Number of hydrogen bonds per surface silanol.[a,b]

System	N_{wat}[c]	N_{met}[d]
C_{30}	0.51_2	0.25_1
C_{18}	0.46_2	0.24_1
C_8	0.38_2	0.28_2
C_1	0.57_2	0.17_2
SiO_2	1.28_1	0.23_1

[a] Subscripts indicate the statistical uncertainty in the final digit.
[b] A hydrogen bond is defined by the following geometric criteria: an oxygen–oxygen distance less than 3.3 Å, an oxygen–hydrogen distance less that 2.5 Å, and a hydrogen bond angle with a cosine less than −0.1 [75].
[c] Number of hydrogen bonds with water.
[d] Number of hydrogen bonds with methanol.

four alkylsilane systems. For the C_1 phase the interface is very sharp and the methanol enrichment is very pronounced. Whereas the total solvent density decays smoothly in the interfacial region in the other alkylsilane systems, for the C_1 phase, it shows an oscillating behavior similar to a fluid in contact with "hard walls" [58–60]. Another difference between the alkylsilane phases is noted for the C_8 phase. Here, the interfacial width is larger than for the other systems, a consequence of more significant solvent penetration in the C_8 stationary phase as compared to the C_{18} and C_{30} stationary phases (see Fig. 4). This effect can understood by examining the simulation snapshots of each system in Fig. 1. It appears the C_8 phase is unable to completely cover the silica surface and filaments of solvent molecules bridging the substrate and mobile-phase region are quite prevalent, whereas the C_{18} and C_{30} phases form a continuous layer with respect to solvent penetration and solvent bridges are extremely rare for the C_{18} phase [14,61]. In other words, the C_8 phase forms a more heterogeneous surface layer. Differences in the lateral diffusion of a nonpolar solute between a C_8 phase and a C_{18} phase have also been observed [62], but the connection between kinetics and structure can be tenuous. It should be noted here that the water and methanol densities in the interior region of the C_{30} phase are about one order of magnitude smaller than the corresponding densities for the C_{18} phase which, in turn, are two and three orders of magnitude smaller than the methanol and water densities in the bulk mobile phase.

The position of the GDS also allows for a quantification of the thickness of the different bonded phases. As one would expect, the value of z_{GDS} increases with increasing chain length. These values are also quite similar to the experimental data of Sander et al. [63], who measured bonded phase thickness by small angle neutron scattering and found values of 25 ± 4, 17 ± 3, and 10 ± 3 Å for C_{30}, C_{18}, and C_8 monomeric phases, respectively, and these values fall within the ranges found in other simulation studies [8,11,14,17].

Moving from the interface to deep within the stationary phase, peaks in the density of the two solvents can be seen around $z \approx 3$ Å. These peaks are indicative of solvent molecules forming direct hydrogen bonds to the residual surface silanols [14,50,61]. These peaks appear to be similar in magnitude for the C_{30}, C_{18}, and C_8 alkylsilane systems, suggesting there is little change in hydrogen bonding at the silica surface as chain length is changed, whereas previous simulation studies indicated a dependence on ligand grafting density and embedded polar groups [18,20]. This is confirmed by an analysis of the number hydrogen bonds per surface silanol (see Table 2), which shows that each silanol forms about 0.7 hydrogen bonds in all four alkylsilane systems. The residual silanols in the C_{30} and C_{18} systems do not show a preference for hydrogen bonding with either solvent species, i.e., they form twice as many hydrogen bonds with water, but there is twice as much water as methanol present in the 33% molfraction methanol solvent. However, it appears that the silanols in the C_1 system exhibit a weak preference for hydrogen-bonding to water, whereas the opposite is observed for the C_8 system.

The density profiles for the bare SiO_2 substrate are significantly different than the alkylsilane phases, i.e., it is a polar surface compared to the nonpolar alkylsilane surfaces. By definition, this would correspond to a HILIC (hydrophilic interaction liquid chromatography) stationary phase [64,65] rather than an RPLC stationary phase. The density profiles for the SiO_2 phase show a high degree of structure near the silica surface, but the profiles decay to bulk behavior within 10 Å of the surface. In this structured region there are three distinct peaks, or layers, in the total solvent density at z values of approximately 3, 5.5, and 8 Å. The first peak, nearest the surface, is highly enriched in water, the second peak is enriched in methanol and reaches the very high density of 1.2 g/mL (compared to the bulk solvent density near 0.8 g/mL), and the third peak is not dramatically enriched in either solvent component and is only slightly higher than the bulk solvent density. This solvent structure is relevant to the retention mechanism on HILIC phases. It is often argued that polar solutes are retained on HILIC phases by partitioning into a water enriched layer atop the stationary phase [64–68]. Our simulation results indicate that there is indeed a water-rich layer near the surface, however this layer is thin ($z = 3$–5 Å) and represents only a monolayer of water rather than an extensive region into which solutes could partition into. However, irrespective of composition enhancements the transport properties in these highly structured solvent layers will be different from those in the bulk liquid solvent [60].

The monolayer of water adsorbed at the silica surface indicates that the surface silanols have a preference to hydrogen bond with water as opposed to methanol. This is confirmed by the hydrogen bond analysis presented in Table 2, which shows that a silanol is over five times more likely to hydrogen bond with water than with methanol. In addition to a preference for water, the silanols on the bare silica surface form about twice as many total hydrogen bonds to solvent when compared to the residual silanols in the alkylsilane systems.

3.1.3. Retention characteristics

For a complete, molecular-level understanding of solute retention one needs to know exactly where the solutes are retained within the stationary phase. To garner this insight, the distribution coefficient for transfer from mobile to stationary phase is plotted as a function of z in Fig. 5 for two solutes, n-butane and 1-propanol. These distribution coefficient profiles, $K(z)$, are computed by dividing the solute's z-dependent density profile by its density in the mobile phase. Thus, larger values of $K(z)$ correspond to more probable z-locations for the solute. It should be noted that this quantity is related to the experimentally measurable distribution coefficient for transfer between two phases, however, $K(z)$ gives much more localized information [43].

In viewing the $K(z)$ profile for n-butane, one sees that retention (i.e., the area under the curves) increases with increasing chain length, which is in agreement with experimental retention data [22–29]. Despite this increase in retention, it appears that the mechanism of retention is similar for the C_8, C_{18}, and C_{30} phases. For the C_{18} and C_{30} phases, the $K(z)$ profiles show a clear bimodal distribution with one peak in the interfacial region just inside the GDS for each system (vertical dashed lines) and one peak deep within the bonded phase ($z \approx 8$ Å). This indicates that the nonpolar alkane solute shows a mixed retention mechanism with contributions from adsorption in the interfacial region and partitioning deep into the stationary phase [15,17]. For the C_8 phase it appears that only one distinct peak in the $K(z)$ profile is present, however this does not rule out a mixed retention mechanism. The location of the single peak for C_8 nearly coincides with the partitioning peak found for the C_{18} and C_{30} phases, but it is also located just inside

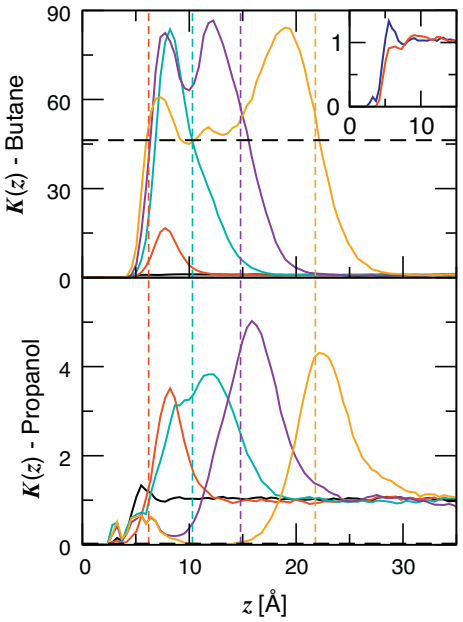

Fig. 5. Distribution coefficient profiles for *n*-butane (top) and 1-propanol (bottom). Black, red, cyan, purple, and orange lines are used to represent the bare silica, C_1, C_8, C_{18}, and C_{30} phases, respectively. The dashed vertical lines indicate the position of the GDS in each system. The dashed horizontal line is used to indicate the value for partitioning in the hexadecane/33M system [16]. The inset shows the distribution coefficient profiles for *n*-butane (red) and 1-propanol (blue) on the bare silica phase. (For interpretation of the references to color in this figure legend, the reader is referred to the web version of the article.)

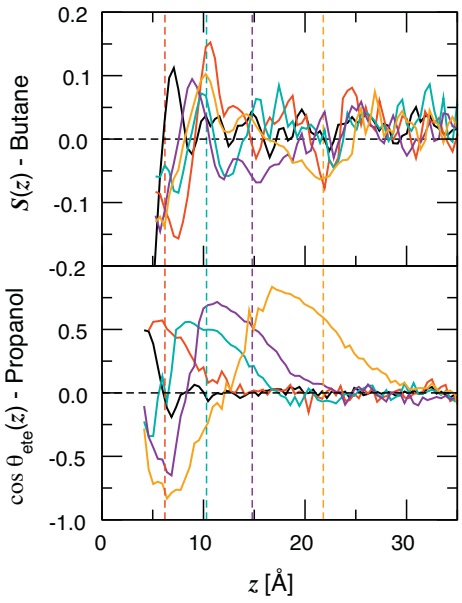

Fig. 6. Solute orientational profiles. Line styles as in Fig. 5.

the GDS for this system and has a shoulder extending into the interfacial region. This suggests that this peak arises from spatially overlapping partition and adsorption contributions.

For the C_1 phase, retention must be dominated by adsorption since the phase is too thin to allow for partitioning and indeed there is only one peak in the $K(z)$ profile. This peak is roughly five times smaller than the peaks in $K(z)$ corresponding to adsorption in the other systems. This indicates that adsorption on a "hard" nonpolar surface (the C_1 surface) is different than adsorption on a more flexible, or "soft", surface (the C_{18} and C_{30} surfaces). Interestingly, the peaks corresponding to adsorption and partitioning on the C_{18} and C_{30} are roughly similar in height. Thus, in terms of free energy, adsorption and partitioning in the these phases is thermodynamically similar. This is in contrast to lattice theories by Dill and Dorsey which indicate that partitioning should be significantly more favorable than adsorption [69,70].

Also noteworthy is a comparison of the $K(z)$ values to the distribution coefficient for transfer from a 33% methanol solvent to liquid hexadecane, i.e., bulk liquid–liquid partitioning [71]. In previous work using the same simulation methodology and force field, but liquid hexadecane instead of an explicit stationary phase, we calculated a partition coefficient of 46.3 for *n*-butane [16]. This value is shown as the horizontal dashed line in Fig. 5. For the C_8, C_{18}, and C_{30} phases, the maxima in $K(z)$ are larger than this value, indicating that those regions of the stationary phase are more favorable than the liquid alkane. However, it appears that an extended region in the center of the C_{30} phase (z = 10–15 Å) behaves very similar to the liquid alkane, at least in terms of solvation thermodynamics.

1-Propanol (a polar solute, but roughly the same size as *n*-butane) shows a similar retention mechanism on all four alkylsilane phases. There is a peak for each phase within the interfacial region, but just outside the GDS. These peaks correspond to adsorption at the interface where 1-propanol can insert its nonpolar tail into the stationary phase while its hydroxyl group is able to hydrogen bond with the mobile phase solvent [15,17]. The interfacial $K(z)$ peak is somewhat broader for the C_8 phase and extends further into the stationary phase. This is likely the result of the increased width of the interfacial region due to increased solvent penetration in the C_8 phase (see Fig. 4 and Table 1). Additional, but much smaller, peaks in the $K(z)$ profile are observed near the silica surface. These peaks result from the hydrogen bonding of the 1-propanol solute with surface silanols and surface bound solvent molecules [15,17]. A further analysis of hydrogen bonding for alcohol solutes will be given below.

Both the polar and nonpolar solute examined here exhibit an anisotropic spatial distribution within the alkylsilane stationary phases. Unlike a liquid, these stationary phases are heterogeneous and there are specific regions where the solutes prefer to be retained. This heterogeneity is further demonstrated by an examination of orientation of the solutes in these preferred retention regions. For this purpose, $S(z)$ profiles for *n*-butane and $\cos\theta_{ete}(z)$ profiles for 1-propanol are shown in Fig. 6. The order parameter S for *n*-butane is the same as that described for the alkyl chains in Eq. (1), except here is it plotted as a function of z. The angle θ_{ete} is measured between the silica surface normal and the end-to-end (ete) vector of the 1-propanol molecules. This end-to-end vector originates at the methyl group and terminates at the hydroxyl hydrogen. Thus, values of $\cos\theta_{ete}$ will be positive for hydroxyl groups pointing away from the silica surface, negative for hydroxyl groups directed towards the surface, and vanish if there is no preferred direction for the hydroxyl group.

In the orientational profiles for *n*-butane, a similar trend is followed on the C_8, C_{18}, and C_{30} phases. Values of $S(z)$ are slightly negative in the interfacial region. This is consistent with an adsorption mechanism where the solutes exhibit some preference to lay parallel to the interface. In the center of the bonded phase at $z \approx 8$ Å, where *n*-butane solutes also showed a peak in the $K(z)$ profile, values of $S(z)$ are slightly positive. This indicates that the solutes are weakly aligned perpendicular to the silica surface, i.e., with the alkyl chains of the stationary phase. Retention in this region of the stationary phase may be classified as partitioning since the solutes are fully embedded into the chains. However, this partitioning does not resemble bulk liquid–liquid partitioning where one would not observe any orientational preference. The alignment of the solute is not surprising since the lower segments of the stationary phase chains also tend to be directed away from the surface (see Fig. 2).

Table 3
Number of hydrogen bonds per alcohol solute molecule retained on the stationary phase.[a,b,c]

System	N_{SiOH}[d]	N_{in}[e]	N_{out}[f]	N_{total}[g]
C_{30}	0.13_1	0.43_1	1.40_1	1.96_1
C_{18}	0.08_2	0.41_3	1.48_2	1.97_2
C_8	0.14_1	0.44_1	1.44_1	2.02_1
C_1	0.07_3	0.17_1	1.79_1	2.03_1
SiO_2	0.30_2	–	1.84_2	2.14_2
Mobile phase[h]				2.17_2
Hexadecane[i]				0.30_8

[a] Subscripts indicate the statistical uncertainty in the final digit.
[b] In the alkylsilane systems a solute is defined to be in the retentive phase when it is inside the first solvation shell (within 6 Å) of any stationary phase CH_x segment and in the bare SiO_2 system if it is within 7.5 Å of the silica surface (i.e., containing the peak in 1-propanol's $K(z)$ profile).
[c] Hydrogen bond definition as in Table 2
[d] Average number of hydrogen bonds with surface silanols.
[e] Average number of hydrogen bonds with solvent molecules inside the GDS.
[f] Average number of hydrogen bonds with solvent molecules outside the GDS.
[g] Total number of hydrogen bonds for solutes inside the stationary phase.
[h] Total number of hydrogen bonds in the bulk mobile phase.
[i] Total number of hydrogen bonds in a bulk *n*-hexadecane phase that is in contact with the mobile phase [16].

For the C_1 phase, the *n*-butane solute shows negative values for $S(z)$ when very close to surface ($z = 5$–7 Å) as it prefers to lie down parallel when the entire molecule adsorbs onto the trimethyl silane groups. The $S(z)$ values are positive at $z \approx 10$ Å, perhaps because the solute has only one of its CH_3 groups adsorbed to the C_1 surface while the remainder of the solute is in the methanol enriched interfacial region.

For 1-propanol, one also sees similar orientational trends on all four alkylsilane phases. Values of $\cos\theta_{ete}(z)$ are positive near the GDS. This indicates that the alkyl tail of 1-propanol is directed towards the stationary phase, while its hydroxyl group is directed towards the solvent and available for hydrogen bonding with solvent molecules. Near the silica surface values of $\cos\theta_{ete}(z)$ become negative indicating that the hydroxyl group is now directed towards the silica surface. In this orientation, 1-propanol molecules can form hydrogen bonds with the residual silanol groups and solvent molecules bound to these groups.

Retention is quite a bit different on the bare SiO_2 phase. For *n*-butane, the $K(z)$ profiles (red line in inset of Fig. 5) show that there is a slight depletion near the silica surface with $K(z)$ values less than one. This nonpolar solute cannot interact with the surface silanols and prefers not to be where the total system density is very high (near $z \approx 6$ Å, see Fig. 4). For 1-propanol (blue line on inset of Fig. 5), there is a very slight enrichment near the silica surface. Thus, as would be expected, the retention order is reversed when comparing the alkylsilane phases to the HILIC phase [64,65]. In terms of orientation, the *n*-butane molecules show negative values of $S(z)$ when very close to the silica surface, but slightly positive values at about $z = 7$ Å. The 1-propanol molecules exhibit slightly positive values $\cos\theta_{ete}(z)$ near the silica surface, indicating that the hydroxyl group is preferentially directed away from the silica surface. This is contrary to the expectation that a 1-propanol molecule would direct its hydroxyl group towards the silica surface so that it could participate in hydrogen bonding with the surface silanols. From this, it appears the solute is interacting more with surface bound solvent than with the silanols themselves.

The retention behavior of 1-propanol on all five stationary phases utilized in this study can be rationalized through an analysis of hydrogen bonding. Table 3 gives the number of hydrogen bonds for alcohol solute molecules that are retained on the stationary phase. For the alkylsilane phases, one sees a striking similarity. The alcohol solutes all form around two hydrogen bonds when retained on the stationary phase, the majority of the hydrogen bonds are

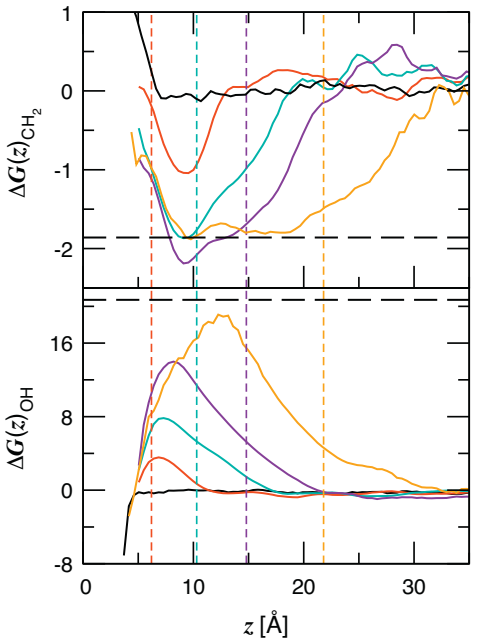

Fig. 7. Incremental free energy profiles. Line styles as in Fig. 5.

to solvent molecules outside the stationary phase, and very few hydrogen bonds are directly to the residual silanols. Thus, the most important contributor to retention for the alcohol solute is adsorption in the interfacial region where the solute's alkyl tail can interact with the stationary phase chains and the hydroxyl group can interact with solvent in the mobile phase. The only significant difference between the alkylsilane phases is the alcohol solute shows very few hydrogen bonds with solvent sorbed in the C_1 stationary phase. This occurs because the C_1 phase has a much smaller volume, so there is a lower probability of interacting with a solvent inside this volume. For the bare SiO_2 phase, the retained alcohol solute has a much larger number of hydrogen bonds to surface silanols than in the alkylsilane phases. However, it forms six times as many hydrogen bonds with solvent molecules than with silanols. Thus, for the HILIC phase, direct interactions with surface silanols do contribute significantly to retention, but interaction with solvent near the surface is more important.

A comparison of the retention characteristics of *n*-butane and 1-propanol, i.e., a nonpolar and a polar solute, were given above. However, further insight on the contribution of nonpolar and polar groups can be gleaned from the incremental free energy profiles for methylene and hydroxyl groups ($\Delta G_{CH_2}(z)$ and $\Delta G_{OH}(z)$) shown in Fig. 7. $\Delta G_{CH_2}(z)$ is computed by converting the $K(z)$ profiles for ethane, propane, and *n*-butane into free energy profiles through the standard relation $\Delta G = -RT\ln K$. A linear regression on the free energy versus number of solute carbons is then performed at each value of z in these profiles. The slope of this regression corresponds to ΔG_{CH_2}. $\Delta G_{OH}(z)$ is found by subtracting the free energy profile for an alkane solute from the free energy profile of an alcohol solute with the same number of carbons.

For each of the alkylsilane phases, $\Delta G_{CH_2}(z)$ shows a minimum (transfer from mobile to stationary phase is most favorable) at $z \approx 9$ Å. The value of this minimum is similar for the C_8, C_{18}, and C_{30} phases, but is roughly half of this magnitude for the C_1 phase. This suggests the molecular origins of this minimum are different for the C_1 phase. At this location a methylene group would be fully embedded in the C_8, C_{18}, and C_{30} phases indicative of partitioning, but this is outside the GDS of the C_1 phase and, therefore, indicative of adsorption. A lower free energy for partitioning than for

adsorption is consistent with the lattice theories of Dill and Dorsey [69,70]. Values of $\Delta G_{CH_2}(z)$ increase, but continue to be negative and favorable as one moves through the interfacial regions of the C_8, C_{18}, and C_{30} phases. Negative $\Delta G_{CH_2}(z)$ values outside the GDS indicate that the nonpolar methylene group can also be retained through adsorption. Again, one sees that the free energy for adsorption on the C_8, C_{18}, and C_{30} phases is lower than the free energy for adsorption on the "hard" C_1 surface.

For a comparison to bulk liquid–liquid partitioning, a horizontal line indicating the methylene increment for transfer from a 33% methanol solvent to *n*-hexadecane is also shown in Fig. 7. Interestingly, there is an extended region in the center of the C_{30} phase for which the methylene increment is flat and very close to the value for hexadecane partitioning. This would suggest a similarity to bulk liquid–liquid partitioning. However, the $S(z)$ profile for *n*-butane indicates orientational preferences in this region of the C_{30} phase and one would not see such preferences in a bulk liquid. It is also noteworthy that the ΔG_{CH_2} value for the hexadecane phase is not much lower than $\Delta G_{CH_2}(z)$ values in the interfacial regions of the C_8, C_{18}, and C_{30} stationary phase. This suggests that comparing free energies of retention to free energies of transfer for bulk liquid–liquid systems may not be useful in discriminating between adsorption and retention mechanisms in RPLC as has been suggested by others [29,69–71].

In the incremental free energy profiles of the polar hydroxyl group, a distinct trend is observed with decreasing chain length. For each of the alkylsilane phases there is a free energy barrier to move from the mobile phase through the stationary phase and to silica surface, where $\Delta G_{OH}(z)$ is negative. This barrier becomes much smaller as chain length is decreased and disappears for the bare SiO_2 phase. In contrast to ΔG_{OH}, ΔG_{CH_2} shows a maximum near the silica surface of the bare SiO_2 phase. No minimum is apparent in $\Delta G_{CH_2}(z)$, so a nonpolar methylene group is completely unretained on the SiO_2 phase.

3.2. Effects of solute length

As mentioned in Section 1, careful experimental measurements have shown a break in the slope of plots of $\log k'$ versus number of carbons for various homologous series (including *n*-alkanes, *n*-alkyl chlorides, methyl esters of linear carboxylic acids, *n*-alcohols, and *n*-alkan-2-ones) at the point where the number of carbons exceeds the stationary phase chain length [27,35]. Stated otherwise, the methylene increment (ΔG_{CH_2}) shows a small increase at this critical carbon number. For example, Tchapla et al. found, for a C_8 stationary phase and a 10/90 (v/v) water/methanol mobile phase, that the methylene increment increased (became less favorable) by 0.1 kJ/mol when the number of carbons in the solute was greater than ten [35]. From this it was suggested that the solutes fully embed themselves (partition) into the stationary phase until their length exceeds the length of the stationary phase and, after this, the remaining portion of the solute is forced to reside outside the stationary phase and adsorb at the surface [27,35]. Indeed, 0.1 kJ/mol is a very small change in transfer free energy to base an argument for a change in the retention mechanism. Since the change in the slope found by Tchapla et al. is about a factor of six smaller than the slope itself, one may actually deduce that the solvation environment for methylene segments of the longer solutes should be much more similar to that experienced by the shorter solutes than to one experienced by a solute in the mobile phase.

The free energies of retention for even-numbered linear alkanes, as a function of solute carbon number computed from the present simulations, are shown in Fig. 8. The slope of this plot corresponds to the methylene increment and is also indicated in the figure. The methylene increment measured by Tchapla et al. [35] on the C_8 phase range from −0.65 kJ/mol for the shorter

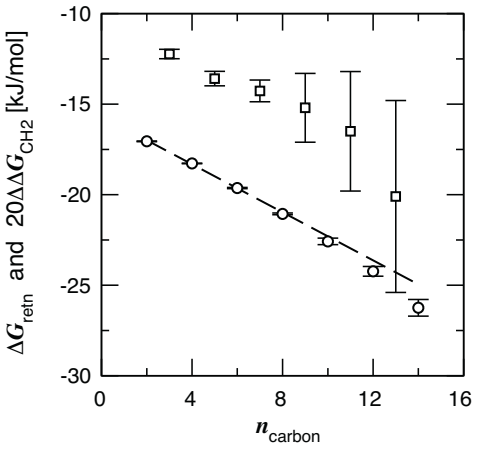

Fig. 8. Free energy of retention, ΔG_{retn}, and methylene increment, $\Delta\Delta G_{CH_2}(n) = 0.5\,[\Delta G_{retn}(n+1) - \Delta G_{retn}(n-1)]$, versus solute carbon number on the C_8 phase are shown as circles and squares, respectively. The dashed line depicts a weighted linear fit of the ΔG_{retn} data and yields a methylene increment of 0.7 kJ/mol.

solutes to −0.53 kJ/mol for the longer solutes, whereas the simulation data range from -0.61 ± 0.02 to -1.0 ± 0.3 kJ/mol and a weighted linear fit yields -0.7 ± 0.1 kJ/mol. It is evident from Fig. 8 that the computed methylene increment does not exhibit a break when the solute carbon number is increased past the number of carbons in the stationary phase chains. On the other hand it appears that the magnitude of the methylene increment is increasing with increasing solute chain length. Although the statistical uncertainties (standard error of the mean) of the free energies of retention computed from the present simulation are very small for the smaller solutes examined (e.g., ±0.02 kJ/mol for ethane), they become significant for the larger solutes (e.g., ±0.4 kJ/mol for tetradecane). As a consequence, the uncertainties in the calculated free energy of the methylene increment are sufficiently large that the difference between the increments calculated from the hexane–butane and dodecane–decane pairs is smaller than the combined uncertainties. Thus, because of this inadequate precision, it is difficult to judge whether the disagreement between the experimental observations of Tchapla et al. [35] and the simulation data is due to inaccuracies in the force field or due to differences in the chromatographic parameters; the simulations were carried out at a higher water content of the mobile phase (20/80 versus 10/90, v/v). Furthermore, the bonding density is not provided by Tchapla et al. and it is possible that a more ordered phase at higher coverage and/or lower temperature would yield different results. Here we should also mention that curvature in the incremental free energy of retention has been observed by Engelhardt and Ahr for a C_6 stationary phase, but again the grafting density is not specified [37].

Despite these ambiguities, an analysis of the spatial and orientational distribution may still be useful for examining the retention mechanism of large, flexible solutes. Distribution coefficients as a function of distance from the silica surface for ethane, *n*-octane, and *n*-tetradecane are presented in Fig. 9. The top part of this figure shows the distribution coefficient profiles, $K(z)$ computed using the center of mass coordinate (COM) of the solutes (see also Fig. 5) [43]. Due to the large size and flexibility of some of the solutes examined here, however, the COM coordinates may not be the best descriptor of solute location. Therefore, normalized distribution profiles, $H(z)$, for the location of the methyl groups (CH_3), the six methylene (CH_2^{oct}) groups of *n*-octane, and the six interior and exterior methylene groups (CH_2^{int} and CH_2^{ext}) of *n*-tetradecane are also shown in Fig. 9. To facilitate comparison of the spatial distribution, the normalization of the $H(z)$ profiles is done in a manner that the integral

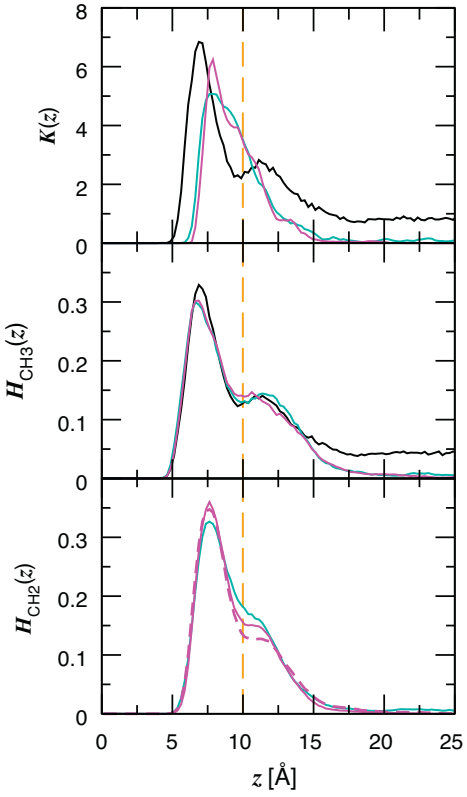

Fig. 9. Distribution profiles for normal alkane solutes of differing length on a C_8 phase. (Top) $K(z)$ profiles; scaled by factors of 10^{-1} and 10^{-2} for *n*-octane and *n*-tetradecane, respectively. (Middle) Normalized distribution profiles for methyl groups. (Bottom) Normalized distribution profiles for methylene groups. Data for ethane, *n*-octane, and *n*-tetradecane are shown in black, cyan, and magenta, respectively. For the methylene groups of *n*-tetradecane, the profiles of the six interior and the six exterior methylene groups are shown as solid and dashed lines, respectively. The dashed vertical line indicates the position of the GDS that is found at $z = 10.0$ Å; a slightly smaller value than for the investigation of the ligand chain length, but temperature and mobile phase composition differ for the two C_8 systems. (For interpretation of the references to color in this figure legend, the reader is referred to the web version of the article.)

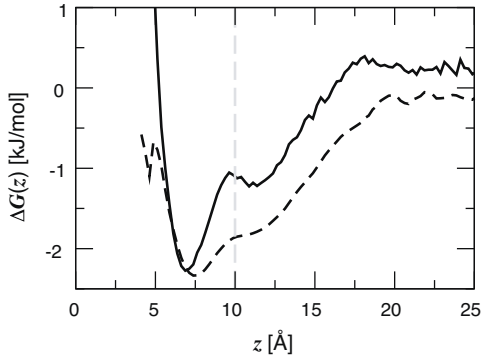

Fig. 10. Profiles for the incremental free energy of transfer of a methylene unit (dashed line) computed from data for solutes ranging from ethane to *n*-tetradecane and half of the free energy of transfer for a methyl unit of ethane (solid line). The dashed vertical line indicates the position of the GDS.

of $H(z)$ from $z = 0$ to the GDS yields a value of unity irrespective of the excess compared to the mobile-phase region.

The $K(z)$ and $H_{CH_3}(z)$ profiles for ethane trace each other very closely and exhibit a clear bimodal distribution with one peak inside the GDS and one peak outside. This close agreement and the fact that the separation between the two peaks is much too large to be explained by the C–C bond length, again support the notion that there are two preferred regions for solute retention. The CH_3 profiles for *n*-octane and *n*-tetradecane also show the bimodal character and are strikingly similar to that for ethane (with the exception of the region of $z > 15$ Å, where $H(z)$ for ethane is much larger due to its higher solubility in the mobile phase). In contrast to the $H_{CH_3}(z)$ profiles, there are significant differences in the shape of the $K(z)$ profiles for these three analytes. The $K(z)$ profiles for the larger analytes are much narrower and the peak found outside the GDS for ethane, has diminished to a weak shoulder located inside the GDS. The narrowing of the $K(z)$ profiles and the close agreement for the $H_{CH_3}(z)$ profiles are an indication that the larger solutes exhibit some preferential alignment with the surface normal (see below) and a given molecule spans its segments over a significant z range. The spatial distributions for the methylene segments are quite similar for *n*-octane and *n*-tetradecane, but $H(z)$ yields slightly smaller values in the region $9\text{ Å} < z < 12\text{ Å}$ for *n*-tetradecane than for *n*-octane ($CH_2^{int} < CH_2^{ext} < CH_2^{oct}$).

The z-dependence of the incremental free transfer free energy for the methylene unit, $\Delta G_{CH_2}(z)$, and of the transfer free energy for the methyl group of ethane, $\Delta G_{CH_3}(z) = -0.5RT \ln K_{CH_3}(z)$ (where the factor of 0.5 takes account of the two methyl groups in a single ethane molecule), are shown in Fig. 10. It should be noted here that $\Delta G_{CH_2}(z)$ differs from the corresponding profile in Fig. 7 because of changes in temperature (298 versus 323 K) and mobile-phase composition (80/20 versus 50/50, v/v). The simulation data from the present work indicate that $\Delta G_{CH_2}(z)$ is slightly less favorable in the interfacial region as compared to the interior region of the bonded phase and decreases in magnitude by ≈0.2 kJ/mol for an outward shift of 1 Å in the interfacial region (see Fig. 10). These shifts in the transfer free energy are in agreement with the outward shift of the methylene units deduced from the experimental data but it needs to be emphasized how little change in the average position of a methylene group would be required for a change of 0.1 kJ/mol in $\Delta G_{CH_2}(z)$. Based on comparison of the z-dependence of the normalized distribution profile and the transfer free energy for the methylene increment (see Figs. 9 and 10), it appears that the methylene segments for *n*-tetradecane are occupying regions of slightly more favorable transfer free energy than those for *n*-octane. This very minor difference may be sufficient to cause the curvature in ΔG as function of chain length. In other words, the simulation data indicate that addition of a methylene group "pulls" the solute deeper into the bonded-phase region toward the location of the minimum in $\Delta G_{CH_2}(z)$.

These observations indicate that large flexible solutes exhibit a tendency to arrange in such a manner that part of the segments are found in the partition region and another part in the adsorption region above the GDS, which is consistent but more nuanced than the suggestion that larger solutes are retained by embedding part of the chain inside of the stationary phase while the remainder of the chain adsorbs at the bonded phase surface [27,35]. However, the microscopic-level information from our simulations does not support the view that the small solutes are only retained by fully embedding themselves (partitioning) into the stationary phase [70–74]. The bimodal COM distribution exhibited by the C_2 solute clearly demonstrates this. At first hand, there appears to be a contradiction between the minimum in $\Delta G_{CH_2}(z)$ at $z \approx 7.5$ Å and a bimodal distribution. The transfer free energy for the methyl group is, of course, only a reflection of this bimodal distribution. The contradiction can be resolved by comparing the average $\Delta\Delta G_{CH_2}(n)$ (see Fig. 8) to the profile of $\Delta G_{CH_2}(z)$ (see Fig. 10). The former is much smaller in magnitude than the minimum in $\Delta G_{CH_2}(z)$, i.e., not all units of an articulated solute can be at an optimal z value due to constraints of the chain topology and the surrounding bonded-phase ligands and units have to occupy a larger z region. Due to the

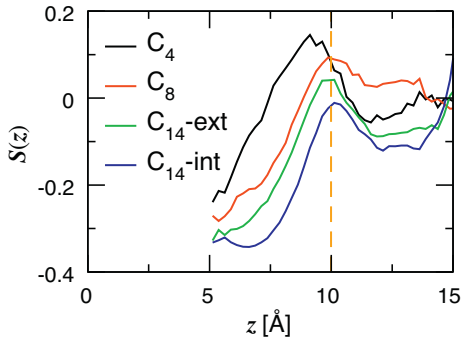

Fig. 11. Orientational profiles for normal alkane solutes of differing length on a C_8 phase. The dashed vertical line indicates the position of the GDS.

asymmetry of $\Delta G_{CH_2}(z)$ and its steep rise for $z < 7$ Å, the center-of-mass of the solute is pushed to larger z values than would be optimal for a single methylene unit. The region just below the GDS is less crowded and allows for placement of multiple units in favorable but not optimal z locations and, hence, there is a significant contribution of adsorption to the overall retention also for the smaller solutes (ethane to *n*-hexane).

Further information on the retention mechanism of these solutes can be seen in the order parameter profiles shown in Fig. 11. The profiles show the order parameter S for the 1–3 backbone vectors of the solute chain plotted as a function of the z-location of the center of the backbone vector. The order parameter profiles are fairly similar in shape regardless of solute size. However, they are shifted downward (more parallel preference) as solute size is increased. For values of $z < 7$ Å, the 1–3 backbone vectors show a preference to be parallel to the silica surface while at the GDS these vectors have a perpendicular preference. Just outside the GDS, the vectors appear to have a slight parallel preference and moving further into the mobile phase they become randomly oriented. Thus, the portions of the alkyl chain that are buried deep inside the stationary phase are somewhat flat relative to the silica surface as they encounter the "wall" created by the dimethyl side chains of stationary phase. Nearer to the ends of the stationary phase chains, solute segments are perpendicular and outside the stationary phase they lie flat against the alkyl surface. These observations are consistent with the suggested mechanism of retention for large solutes [27,35], but inconsistent with a pure partition mechanism for small solutes.

A representative snapshot for a retained C_{14} solute is shown in Fig. 12. The location of this chain is consistent with the distribution coefficient profiles shown in Fig. 9; i.e., the COM of the solute is at about $z = 8$ Å and the CH_3 groups are bimodally distributed with one inside the stationary phase and one at the surface. Consistent with the order parameter profiles, the portion of the chain nearest the silica substrate is aligned parallel to the substrate as it encounters the dimethyl side chains, the interior portion of the solute inside the stationary phase is aligned more toward the surface normal, and the portion of the solute outside the stationary phase is lying flat atop the alkyl surface.

4. Conclusions

When comparing C_8, C_{18}, and C_{30} stationary phases, one sees more similarities than differences. Indeed, one finds that smaller chains are more conformationally disordered, but more aligned. However, larger changes in chain structure were observed for simulations of C_{18} stationary phases with different surface coverages [18]. Furthermore, the retention mechanisms of nonpolar and polar solutes exhibit the same qualitative features for C_8, C_{18}, and C_{30} bonded phases. For nonpolar solutes the retention mechanism is a mix of adsorption at the chain surface and partitioning inside the chain structure. For polar solutes the retention mechanism is dominated by adsorption at the chain surface, but there are minor contributions from interactions with the surface silanols and their bound solvent. The retention mechanism is different for nonpolar solutes on the C_1 phase where a pure adsorption mechanism is observed since the C_1 phase is too thin to allow for partitioning. Additionally, adsorption of nonpolar solutes at the more rigid C_1 surface is thermodynamically less favorable than adsorption on the alkyl surface of longer, more flexible chains.

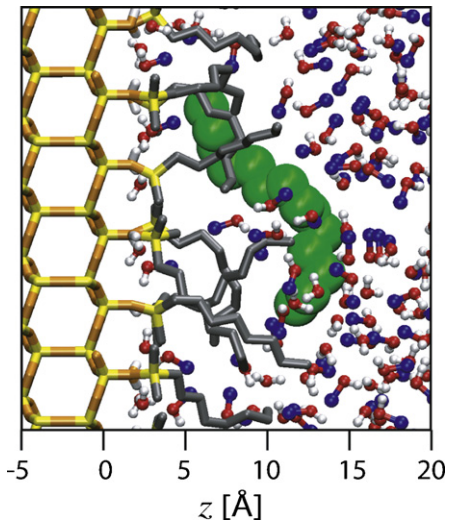

Fig. 12. Snapshot of a C_{14} alkane solute retained on the C_8 phase. The large analyte spans the partition and adsorption regions found for the retention of small analytes.

As to be expected, the polar surface of bare SiO_2 phase studied here behaves differently than the hydrophobic alkylsilane surfaces. At the silica surface there is a high degree of solvent structure with distinct layers of solvent. Only the first layer is found to be enriched in water, rather than an extended water-riched region as suggested for HILIC phases. However, the high degree of structuring in these layers is likely consistent with much slower transport properties. Nonpolar alkane solutes are unretained on the SiO_2 phase, while alcohol solutes are retained on the surface by hydrogen bonding with surface silanols and surface bound solvent.

The proposed mechanism of retention for large flexible solutes based on experimental retention data [27,35] appears to be qualitatively correct. Larger alkanes partially embed themselves in the stationary phase while a portion of the solute is adsorbed at the stationary/mobile interface. Small solutes are not retained solely by a partition mechanism, rather they also show a mixed adsorption/partition mechanism. Thus, for flexible nonpolar solutes, the retention mechanism does not change significantly with solute size. The only difference is that, due to their length, large, flexible, nonpolar solutes can exhibit both adsorption and partition simultaneously. It is likely that this microscopic description may need adjustment for stationary phases at higher coverage, where the ligands are more ordered, and for solutes with a highly polar functional group, where the strong preference for this group to be well-solvated by the mobile phase leads to an orientational ordering for the solute.

Acknowledgements

Financial support from the National Science Foundation (CHE-0718383). Part of the computer resources were provided by the Minnesota Supercomputing Institute.

References

[1] P.W. Carr, D.E. Martire, L.R. Snyder, J. Chromatogr. A 656 (1993) 1.
[2] M.R. Schure, in: J.J. Pesek, I.E. Leigh (Eds.), Chemically Modified Surfaces, Royal Society of Chemistry, Cambridge, 1994, p. 181.
[3] S.J. Klatte, T.L. Beck, J. Phys. Chem. 97 (1993) 5727.
[4] S.J. Klatte, T.L. Beck, J. Phys. Chem. 100 (1996) 5931.
[5] T.L. Beck, S.J. Klatte, in: J.F. Parcher, T.L. Chester (Eds.), Unified Chromatography, ACS Symposium Series, vol. 748, American Chemical Society, Washington, DC, 2000, p. 67.
[6] I. Yarovsky, M.-I. Aguilar, M.T.W. Hearn, Anal. Chem. 67 (1995) 2145.
[7] I. Yarovsky, M.T.W. Hearn, M.-I. Aguilar, J. Phys. Chem. B 101 (1997) 10962.
[8] J.T. Slusher, R.D. Mountain, J. Phys. Chem. B 103 (1999) 1354.
[9] K. Ban, Y. Saito, K. Jinno, Anal. Sci. 20 (2004) 1403.
[10] C.F. Zhao, N.M. Cann, J. Chromatogr. A 1149 (2007) 197.
[11] A. Fouqueau, M. Meuwly, R.J. Bemish, J. Phys. Chem. B 111 (2007) 10208.
[12] J. Braun, A. Fouqueau, R.J. Bemish, M. Meuwly, Phys. Chem. Chem. Phys. 10 (2008) 4765.
[13] S.M. Melnikov, A. Höltzel, A. Seidel-Morgenstern, U. Tallarek, J. Phys. Chem. C 113 (2009) 9230.
[14] L. Zhang, J.L. Rafferty, J.I. Siepmann, B. Chen, M.R. Schure, J. Chromatogr. A 1126 (2006) 219.
[15] J.L. Rafferty, L. Zhang, J.I. Siepmann, M.R. Schure, Anal. Chem. 79 (2007) 6551.
[16] J.L. Rafferty, L. Sun, J.I. Siepmann, M.R. Schure, Fluid Phase Equil. 290 (2010) 25.
[17] J.L. Rafferty, L. Sun, J.I. Siepmann, M.R. Schure, J. Chromatogr. A 1218 (2011) 2203.
[18] J. Rafferty, J. Siepmann, M. Schure, J. Chromatogr. A 1204 (2008) 11.
[19] J. Rafferty, J. Siepmann, M. Schure, J. Chromatogr. A 1204 (2008) 20.
[20] J.L. Rafferty, J.I. Siepmann, M.R. Schure, Anal. Chem. 80 (2008) 6214.
[21] J.L. Rafferty, J.I. Siepmann, M.R. Schure, J. Chromatogr. A 1216 (2008) 2320.
[22] J.E.J. Kikta, E. Grushka, Anal. Chem. 48 (1976) 1098.
[23] K. Karch, I. Sebestian, I. Halász, J. Chromatogr. 122 (1976) 3.
[24] K.K. Unger, N. Becker, P. Roumeliotis, J. Chromatogr. 125 (1976) 115.
[25] P. Roumeliotis, K.K. Unger, J. Chromatogr. 149 (1978) 211.
[26] M.C. Hennion, C. Picard, M. Caude, J. Chromatogr. 166 (1978) 21.
[27] G.E. Berendsen, L. de Galan, J. Chromatogr. 196 (1980) 21.
[28] N. Tanaka, K. Sakagami, M. Araki, J. Chromatogr. 199 (1980) 327.
[29] L.C. Tan, P.W. Carr, J. Chromatogr. A 775 (1997) 1.
[30] L.C. Sander, S.A. Wise, Anal. Chem. 59 (1987) 2309.
[31] Z. Liao, C.J. Orendorff, L.C. Sander, J.E. Pemberton, Anal. Chem. 78 (2006) 5813.
[32] Z. Liao, J.E. Pemberton, Anal. Chem. 80 (2008) 2911.
[33] S. Singh, J. Wegmann, K. Albert, K. Müller, J. Phys. Chem. B 106 (2002) 878.
[34] L.C. Sander, K.A. Lippa, S.A. Wise, Anal. Bioanal. Chem. 382 (2008) 646.
[35] A. Tchapla, H. Colin, G. Guiochon, Anal. Chem. 56 (1984) 621.
[36] A. Tchapla, S. Heron, H. Colin, G. Guiochon, Anal. Chem. 60 (1988) 1443.
[37] H. Engelhardt, G. Ahr, Chromatographia 14 (1981) 227.
[38] J.I. Siepmann, D. Frenkel, Mol. Phys. 75 (1992) 59.
[39] T.J.H. Vlugt, M.G. Martin, B. Smit, J.I. Siepmann, R. Krishna, Mol. Phys. 94 (1998) 727.
[40] M.G. Martin, J.I. Siepmann, J. Phys. Chem. B 103 (1999) 4508.
[41] C.D. Wick, J.I. Siepmann, Marcomolecules 33 (2000) 7207–7218.
[42] A.Z. Panagiotopoulos, N. Quirke, M. Stapleton, D.J. Tildesley, Mol. Phys. 63 (1988) 527.
[43] J.L. Rafferty, J.I. Siepmann, M.R. Schure, in: E. Grushka, N. Grinberg (Eds.), Advances in Chromatography, vol. 48, Marcel Dekker, New York, 2010, p. 1.
[44] W.L. Jorgensen, J. Chandrasekhar, J.D. Madura, R.W. Impey, M.L. Klein, J. Chem. Phys 79 (1983) 926.
[45] T.J.H. Vlugt, W. Zhu, F. Kapteijn, J.A. Moulijn, B. Smit, R. Krishna, J. Am. Chem. Soc. 120 (1998) 5599.
[46] E. Demiralp, T. Çağin, W.A. Goddard, Phys. Rev. Lett. 82 (1999) 1708.
[47] B. Chen, J.J. Potoff, J.I. Siepmann, J. Phys. Chem. B 105 (2001) 3093.
[48] M.G. Martin, J.I. Siepmann, J. Phys. Chem. B 102 (1998) 2569.
[49] M.P. Allen, D.J. Tildesley, Computer Simulation of Liquids, Oxford University Press, Oxford, 1987.
[50] L. Zhang, L. Sun, J.I. Siepmann, M.R. Schure, J. Chromatogr. A 1079 (2005) 127.
[51] L. Sun, J.I. Siepmann, M.R. Schure, J. Phys. Chem. B 110 (2006) 10519.
[52] A. Seelig, J. Seelig, Biochemistry 13 (1974) 4839.
[53] A. Zangwill, Physics at Surfaces, Cambridge University Press, Cambridge, UK, 1988.
[54] A.W. Adamson, A.P. Gast, Physical Chemistry of Surfaces, 6th edition, Wiley-Interscience, New York, 1997.
[55] J.W. Cahn, J.E. Hilliard, J. Chem. Phys. 28 (1958) 258.
[56] K. Lum, D. Chandler, J.D. Weeks, J. Phys. Chem. B 103 (1999) 4570.
[57] Y.V. Kazakevich, R. LoBrutto, F. Chan, T. Patel, J. Chromatogr. A 913 (2001) 75.
[58] J. Mittal, J.R. Errington, T.M. Truskett, J. Chem. Phys. 126 (2007) 244708.
[59] D. Argyris, D.R. Cole, A. Striolo, Langmuir 25 (2009) 8025.
[60] D. Argyris, D.R. Cole, A. Striolo, J. Phys. Chem. C 113 (2009) 19591.
[61] M. Orzechowski, M. Meuwly, J. Phys. Chem. B 114 (2010) 12203.
[62] R.L. Hansen, J.M. Harris, Anal. Chem. 68 (1996) 2879.
[63] L.C. Sander, C.J. Glinka, S.A. Wise, Anal. Chem. 62 (1990) 1099.
[64] A.J. Alpert, J. Chromatogr. 499 (1990) 177d.
[65] P. Hemstrom, K. Irgum, J. Sep. Sci. 29 (2006) 1784.
[66] Y. Guo, S. Gaiki, J. Chromatogr. A 1074 (2005) 71.
[67] D.V. McCalley, J. Chromatogr. A 1171 (2007) 46.
[68] D.V. McCalley, U.D. Neue, J. Chromatogr. A 1192 (2008) 225.
[69] K.A. Dill, J. Phys. Chem. 91 (1987) 1980.
[70] J. Dorsey, K.A. Dill, Chem. Rev. 89 (1989) 331.
[71] P.W. Carr, J. Li, A.J. Dallas, D.I. Eikens, L.T. Tan, J. Chromatogr. A 656 (1993) 113.
[72] D.E. Martire, R.E. Boehm, J. Phys. Chem. 87 (1983) 1045.
[73] K.B. Sentell, J.G. Dorsey, Anal. Chem 61 (1989) 930.
[74] R. Tijssen, P.J. Shoenmakers, M.R. Böhmer, L.K. Koopal, H.A.H. Billiet, J. Chromatogr. A 656 (1993) 135.
[75] J.M. Stubbs, J.I. Siepmann, J. Am. Chem. Soc. 127 (2005) 4723.